Journal of the Korean Chemical Society
2017, *Vol. 61, No. 2*
Printed in the Republic of Korea
https://doi.org/10.5012/jkcs.2017.61.2.57

The Phase Transition and Thermochromic Characteristics of W/Mg-codoped Monoclinic VO_2 Nanoparticle and Its Composite Film

Heesun Park, Jongmin Kim, Young Hee Jung†, and Yeong Il Kim*
*Department of Chemistry, Pukyong National University, Busan 48513, Korea. *E-mail: ykim@pknu.ac.kr*
†Research Laboratory, Mapro, Inc. Hanlim, Gimhae, Korea.
(Received February 8, 2017; Accepted February 13, 2017)

ABSTRACT. Monoclinic VO_2(M) nanoparticles codoped with 1.5 at. % W and 2.9 at. % Mg were synthesized by the hydrothermal treatment and post-thermal transformation method of V_2O_5-$H_2C_2O_4$-H_2O with Na_2WO_4 and $Mg(NO_3)_2$. The composite thin film of the W/Mg-codoped VO_2(M) with a commercial acrylic block copolymer was also prepared on PET substrate by wet-coating method. The reversible phase transition characteristics of the codoped VO_2(M) nanoparticles and the composite film were investigated from DSC, resistivity and Vis-NIR transmittance measurements compared with the undoped and W-doped VO_2(M) samples. Mg-codoping into W-doped VO_2(M) nanoparticles synergistically enhanced the transition characteristics by increasing the sharpness of transition while the transition temperature (T_c) lowered by W-doping was maintained. The codoped composite film showed the prominently enhanced NIR switching efficiency compared to only W-doped VO_2(M) film with a lowered T_c.

Key words: Monoclinic VO_2, Thermochromic, Semiconductor-to-metal phase transition, W/Mg-codoping, NIR switching efficiency

INTRODUCTION

Vanadium dioxide of monoclinic M1 phase, VO_2(M), has recently redrawn much attention for the practical application to energy–saving smart window because of its thermochromic property that can control the transmission of infrared (IR) radiation depending on temperature[1]. VO_2(M) undergoes a reversible crystal phase transition from monoclinic to rutile and vice versa at about 68 °C and concomitantly its electrical property changes from semiconducting or insulating to metallic.[2] This transition switches its optical property from IR-transparent at low temperature to IR-reflective at high temperature, which is very useful for modulating solar flux depending on outside temperature. There are many methods for fabricating VO_2 film such as chemical vapor deposition (CVD),[3,4] sol-gel method,[5,6] sputtering deposition,[7] etc. The most cost-effective method among them is the wet-coating method utilizing sol-gel coating solutions. The traditional sol-gel method uses a precursor solution that can be transformed to a target material after heat-treatment. In this method high temperature treatment cannot be usually avoided. In that case it cannot be applied to a plastic substrate such as polyethylene terephthalate (PET) film. The most practical method for preparing thin film on plastic substrate is to utilize coating solution that has well-dispersed target nanoparticles in solvent with matrix polymer.

The transition temperature (T_c) of pure VO_2(M) is too high to be suitable for real-life solar modulation. For the practical purpose it must be lowered down to about room temperature. A number of investigations showed that the cation substitution could change T_c and the room temperature crystal structure.[8] The dopants such as W^{6+}, Nb^{5+} and Mo^{6+} decreased T_c, while the cations such as Ti^{4+}, $Cr^{3+}$and Al^{3+} increased T_c. The tungsten was known to be the most effective dopant to reduce T_c with a rate of about 20 °C per atomic (at.) %.[9] Doping of a certain amount of W into VO_2(M) lowered the transition temperature down to practical one lower than 30 °C but the visible transmittance was still low and the IR transmittance difference after transition became much smaller than the undoped one.[9(c)] The doping of fluorine[10] and magnesium[11] improved the visible transmittance and decrease T_c of VO_2(M) thin films. But F-doping is not suitable for smart window application because the hysteresis became substantially wider. The Mg-doping decreased T_c by ~3 °C per at. % Mg and the transmittance of visible light and solar radiation were enhanced by about 10 % when Mg content was ~7 at. %. The codoping of two different cations were also more interested in. The thin films of W/Mo-, W/Ti-, and W/F-codoped VO_2(M) were investigated by several researchers[12] but an noticeable improvement was not found. Very recently Wang et al. investigated the thermochromic properties of W/Mg-codoped VO_2 thin films that were prepared by the traditional sol-gel method utilizing the precursor solution and

dip coating.[13] They showed a synergistic effect of the codoping by reducing T_c and simultaneously increasing visible transmittance. The synthesis of W/Mg-codoped VO_2(M) nanoparticles has not been reported yet and as mentioned earlier, the better method for preparing thin films on any kind of substrates cost-effectively at low-temperature is another wet-coating method that utilizes the coating solution mixed with nanoparticles of target material and matrix polymer in solvents. Therefore, in order to investigate the synergistic effect of W/Mg-codoping in VO_2(M) further, we have first prepared W/Mg-codoped VO_2(M) nanoparticle by hydrothermal and post thermal treatment method and the transition property was investigated comparatively with undoped and W-doped ones. And then we have prepared the thin composite film of W/Mg-codoped one with polyacrylic block copolymer on PET substrate by the wet-coating method and its thermochromic property was also comparatively investigated.

EXPERIMENTAL

Materials

V_2O_5 (99.2%, Alfa-Aesar) and anhydrous oxalic acid ($H_2C_2O_4$, 95%, Kanto Chemical) were used as vanadium precursor and reducing agent, respectively. Sodium tungstate ($NaWO_4 \cdot 2H_2O$, 99%) and magnesium nitrate ($Mg(NO_3)_2 \cdot 6H_2O$, 99%) that were used as doping agents were obtained from Sigma-Aldrich and Junsei Chemical, respectively. Ethyl acetate (99.5%), ethyl cellosolve (99%) and methyl isobutyl ketone (99.5%) that were used as solvents for coating solution were purchased from Samchun and Junsei. The acrylic block copolymer EFKA 4310 that was employed as dispersing agent and binder was purchased from BASF. Polyethylene terephathate (PET) film with thickness of 50 μm and 0.7% haze was purchased from Kolon industries Inc. Water was purified to 18.1 MΩcm with Barnstead Nanopure water purification system.

Instrumentation

The X-ray diffraction (XRD) patterns were carried out on Phillips X'Pert-MPD diffractometer using Cu Kα radiation source at a scan rate of $0.02^o\ s^{-1}$ in the 2θ range of 5-80°. The morphologies of the samples were characterized by field-emission scanning electron microscope (FE-SEM, Jeol JEM-6700F) and field-emission transmission electron microscope (FE-TEM, Jeol JEM-2100F). The electrical resistance according to temperature change were measured by preparing pellet samples using 4-point probe method. The pellet samples were prepared by applying the pressure of 4.42 MPa to 10 mm pellet die loaded with about 0.1 g of the sample powders. The pellet samples were placed on the electrically insulated plate of which temperature was controlled by heating element and chilling circulator. The pellet samples were contacted with 4-probe with an interval of 1 mm and the resistivity was measured by constant-current mode using Keithley 2400 source meter. Thickness of pellet samples were measured by a microcaliper in order to calibrate thickness. Differential scanning calorimetry (DSC, Perkin-Elmer Pyris 1) was used to measure the phase transition temperature of sample powders with a heating rate of 5 °C/min in nitrogen atmosphere. UV-Vis-NIR spectrophotometer (JASCO V-670) equipped with a Peltier thermostatted sample holder (JASCO ETCS-761) was used to characterize the optical switching properties of VO_2 composite films below and above the phase transition temperature (20-90 °C). Auto film applicator (BMS Tech VT-300D) was used to prepare thin film samples on PET by wet-coating. The amounts of W and Mg in doped VO_2(M) were analyzed with X-ray fluorescence spectrometer (Shimadzu XRF-1700) and atomic absorption spectrometer (Jena Vario 6).

Synthesis of VO_2(B) and VO_2(M)

For VO_2(B), typically 0.04 mol of $H_2C_2O_4$ and 0.02 mol of V_2O_5 were mixed into 50 ml of deionized water at 60-70 °C. The mixture was kept stirred for 24 hours until it turned to blue suspension. The blue suspension was transferred into a 100 ml stainless steel autoclave with Teflon liner and kept in a forced convection oven at 200 °C for 24 hours. After being cooled down to room temperature, the precipitate was filtered and washed thoroughly with water and ethanol, and then dried at 60 °C for 10 hours in air. For the doping of W and Mg into VO_2(B) the appropriate amounts of 1.0 M Na_2WO_4 and $Mg(NO_3)_2$ solutions (W = 1.5 at. %, Mg = 4.5 at. % vs V) were added to the mixed suspension of $H_2C_2O_4$ and V_2O_5 and kept stirred for 24 hours before the hydrothermal treatment. In order to obtain VO_2(M) the synthesized VO_2(B) was heated in a tube furnace under the flow of argon in 80 mL/min as a protective gas at 500 °C for 2 hours, and cooled down to room temperature in the argon flow.

Preparation of thin films of VO_2(M) on PET substrate

1.3 g of pure or doped VO_2(M) powder was dispersed in 8.2 g of the mixed solvent of ethyl acetate, ethyl cellosolve and methyl isobutyl ketone (1:2.5:2 weight ratio) with 0.5 g of an commercial acrylic block copolymer (EFKA 4310) as dispersing agent and the mixture was ball-milled for 8 days. Using this mixed solution as coating solution, the

film of VO_2 was prepared on PET substrate using an auto film applicator equipped with #3 Meyer bar in the rate of 20 mm/s. The cast film of VO_2(M) was dried at room temperature in air. The thickness of the coated films that was measured by alpha-step profiler was about 150 nm in all cases.

RESULTS AND DISCUSSION

In order to prepare VO_2(M) nanoparticles we have synthesized metastable monoclinic VO_2(B) first by the hydrothermal reaction of the precursor solutions of V_2O_5-$H_2C_2O_4$-H_2O system at 200 °C. The direct hydrothermal synthesis of VO_2(M) strongly depended upon the several synthetic conditions such as molar ratio and concentration of precursors, pH, temperature, reaction time and other additives.[14] However, VO_2(B) could be easily prepared from the hydrothermal treatment of V_2O_5-$H_2C_2O_4$-H_2O system whether Na_2WO_4 and $Mg(NO_3)_2$ were included as dopant precursors or not if the reaction temperature was kept near 200 °C.[15] In this study we kept the doping level of W to be 1.5 at. % vs V because 1.5–2 at. % was known to be an appropriate doping level at which a noticeable phase transition could be observable with T_c lowered close to room temperature as mentioned in Introduction.[9a] The doping amounts of W and Mg were analyzed as 1.5 and 2.9 at. % vs V, respectively when the feeding amounts of W and Mg were 1.5 and 4.5 at. %. This means that all fed W in this amount were doped while the fed Mg were partly doped. *Fig.* 1(a) shows the XRD patterns of the W-doped and W/Mg-codoped VO_2(B) compared with the undoped one. Regardless of doping, all three samples showed the well-defined crystal structure of VO_2(B).[16] The peak intensities were all similar in all three cases, which means that doping of W and Mg did not influence on their B phase crystallinity in this doping level. Those VO_2(B)s were transformed to VO_2(M) when they were annealed at 500 °C in an inert condition as shown in *Fig.* 1(b).[17] The well-defined M phase crystal structure was shown in all three cases although VO_2(B) phase was shown in impurity level (indicated as the arrows in *Fig.* 1b) for both the doped cases whereas the undoped was not. Interestingly, the peak intensity and width of both the doped ones were smaller and broader than those of the undoped one. This means that the dopings make the transformation a little difficult and that is why the impurity level of B phase were also shown in both the doped cases. The enlarged (011) peaks of those VO_2(M) were shown in *Fig.* 2. W-doping shifted the peak to lower position and increased the interplanar distance because of

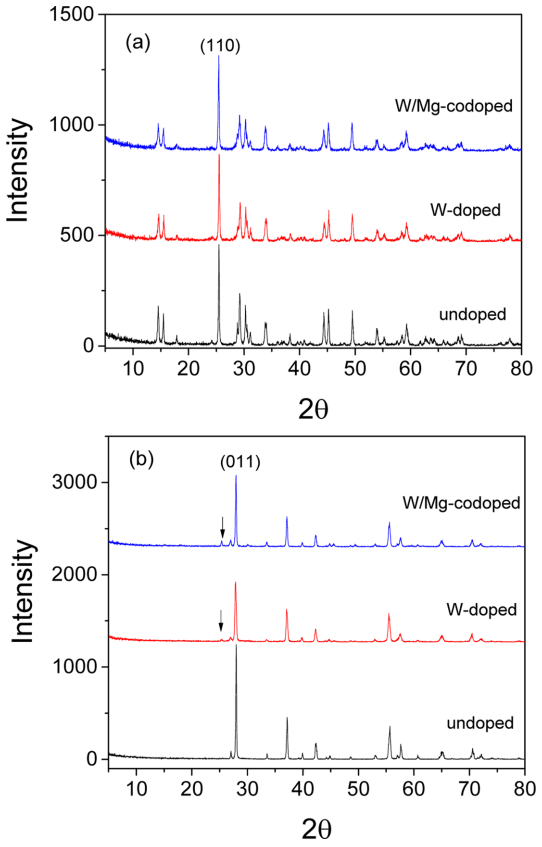

***Figure* 1.** XRD patterns of (a) B and (b) M phases of the undoped, W-doped and W/Mg-codoped VO_2 (The arrows in (b) indicate (110) peak of B phase).

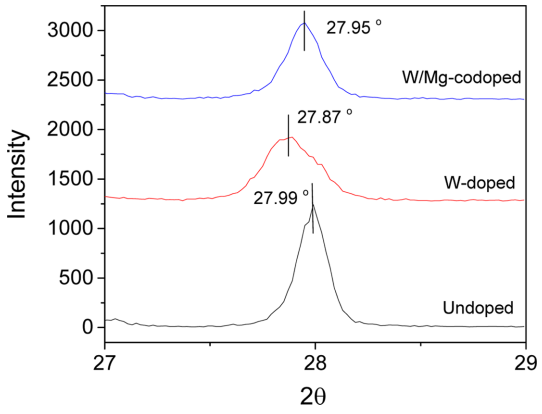

***Figure* 2.** The enlarged (011) peaks of XRD patterns of the undoped, W-doped and W/Mg-codoped VO_2(M).

the larger W atomic size and perturbed the crystallinity to give a broader peak. However, the codoping of W and Mg shifted the peak position back to the undoped and also slightly increased the crystallinity. The crystalline sizes of those VO_2(B) and VO_2(M) that were estimated from (110) and (011) peaks, respectively by applying Debye-Scherrer

***Table* 1.** The crystalline sizes of B and M phases of the undoped, W-doped and W/Mg-codoped VO_2 estimated from the XRD peaks of (110) and (011) planes

	Crystalline size (nm)		
	Undoped	W-doped	W/Mg-codoped
VO_2(B)	52	45	44
VO_2(M)	52	27	43

equation were listed in *Table* 1. For the B-phase samples the sizes of W-doped and W/Mg-codoped ones were not different as estimated to be about 45 nm but when they were transformed to M-phase, the W-doped one became much smaller to 27 nm while the undoped and W/Mg-codoped ones were barely changed. FE-SEM images in *Fig.* 3 depict the morphologies of all the undoped, W-doped and W/Mg-codoped VO_2 powders in B and M phases. In the case of B phase all three samples have a rod-like shape with a similar dimension of about 1 mm length and 200 nm width. When they were transformed to M phase, the morphologies were changed from rod shape to spherical-like one with slight different sizes. The undoped one had the largest size while the W-doped one had the smallest in this aggregated phase. This tendency is consistent with their

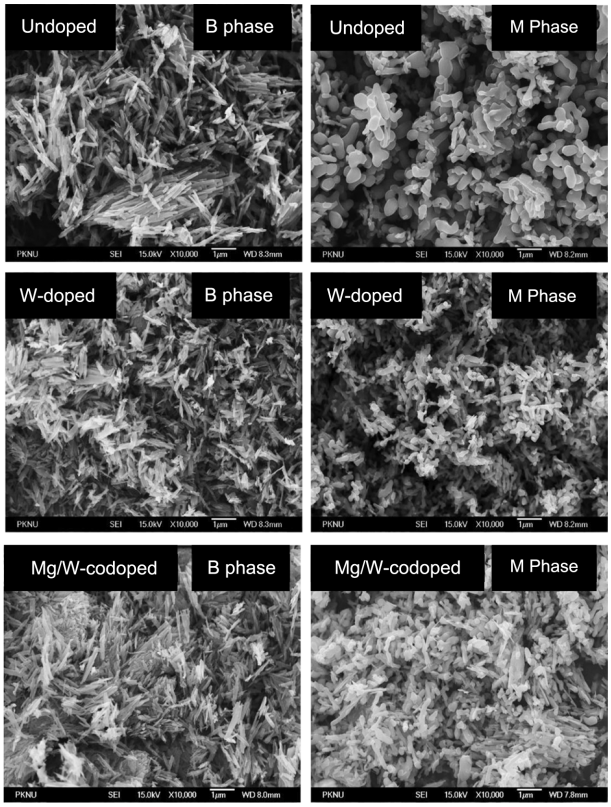

***Figure* 3.** FE-SEM images of B and M phases of the undoped, W-doped and W/Mg-codoped VO_2 (Magnification: x10,000).

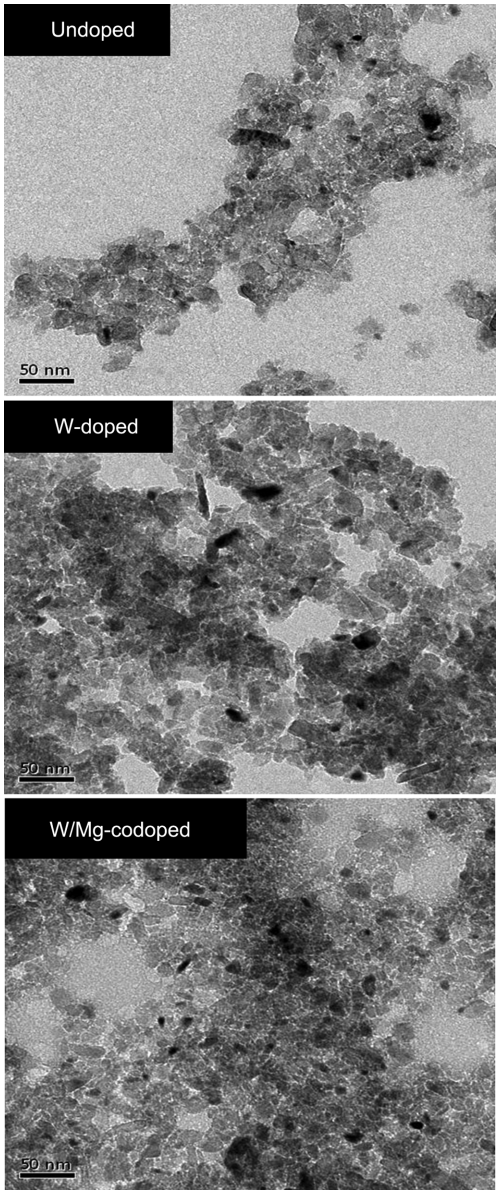

***Figure* 4.** FE-TEM images of the undoped, W-doped and W/Mg-codoped VO_2(M) after being ball-milled in ethanol (Magnification x50,000).

crystalline sizes that were estimated from XRD peaks. When the particles were ball-milled in the solvent to prepare the coating solutions for their thin films, the aggregated particles were broken down to 20–30 nm sizes as shown in FE-TEM images of *Fig.* 4.

The phase transitions of these nanoparticle samples were comparatively characterized by DSC and shown in *Fig.* 5. All three samples showed the noticeable endothermic and exothermic peaks for the heating and cooling cycles, respectively. The transition temperatures that were determined as the average peak temperature for heating and cooling

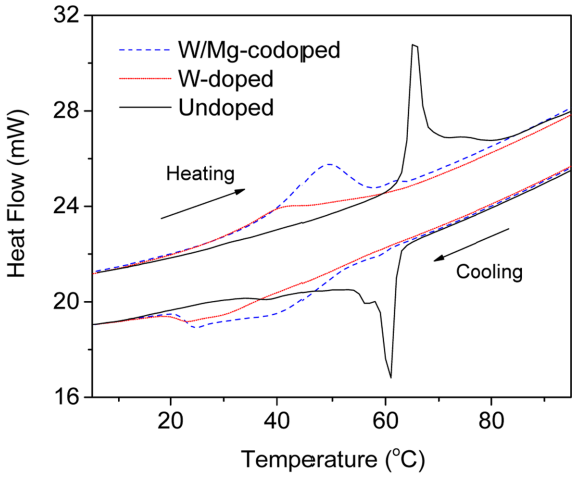

***Figure* 5.** DSC curves of the undoped, W-doped and W/Mg-codoped VO_2(M) (The positive heat flow indicates endothermic reaction).

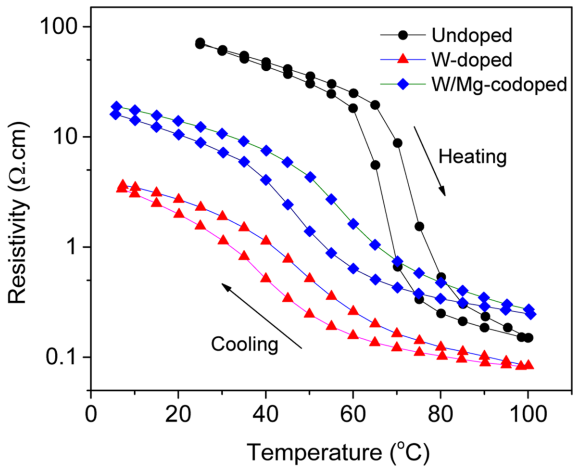

***Figure* 6.** Resistivity-vs.-temperature curves of the pellet samples of the undoped, W-doped and W/Mg-doped VO_2(M).

cycles were 63, 35, 44 °C for the undoped, W-doped, W/Mg-codoped ones, respectively. While the undoped sample showed the sharp peak with small broad shoulder, both the doped ones showed much broader peaks. T_c of the undoped was slightly smaller than the known value in single crystal phase, 68 °C and the hysteresis was relatively narrow. W-doping of 1.5 at. % reduced T_c at the rate of 19 °C per W at. % slightly smaller than the reported rates[18] and made the transition to occur at much broader temperature range. The reduction of T_c by doping of W was firstly explained by Tang *et al*.[9b] According to their explanation, V^{3+}-W^{6+} and V^{3+}-V^{4+} pairs were formed and the loss of direct bonding between V^{4+}-V^{4+} lowered T_c. The widened hysteresis of both the doped samples might be explained by their smaller crystalline sizes than that of the undoped one according to Lopez's nucleation theory.[19] The W/Mg-codoped sample showed slightly higher T_c and narrower hysteresis than those of W-doped one. This means that Mg-codoping into W-doped VO_2(M) turned the transition property slightly back to the undoped one. This is coincident with the crystallinity change shown in XDR data. Mg-doping into VO_2(M) was known to decrease T_c and increase visible transmittance due to the increased unit cell volume and band gap widening as mentioned in Introduction.[11] As far as T_c is concerned, our result showed that Mg-codoping effect into W-doped VO_2(M) was opposite to that of only Mg-doping.

The electrical properties of the undoped, W-doped and W/Mg-codoped VO_2(M) were also studied by preparing the pellet samples of them. The electrical resistivity vs temperature curves for these pellet samples were presented in *Fig.* 6. The resistivity change due to the phase transition was the largest for the undoped one while it was smaller in almost an order of magnitude for both the W-doped and W/Mg-codoped ones. However, the resistivity value of W/Mg-codoped one was higher in about half an order of magnitude than that of W-doped one. W-doping definitely increases the conductivity of VO_2(M) by increasing the carrier concentration as well known. The effect of Mg-doping on T_c and the optical transmittance of VO_2(M) was investigated as mentioned above but not on the electrical conductivity yet as far as we know. The slight increase of resistivity of the W/Mg-codoped one might be explained by the widened band gap as explained in Mg-doped VO_2(M). The bad gap widening will slightly decrease the carrier concentration in the semiconductor. The transition temperatures that were estimated from resistivity measurements also showed the same tendency as that from DSC although the values were slightly higher. In *Table* 2 the phase transition properties were listed comparatively from DSC and resistivity measurements for those undoped, W-doped and W/Mg-codoped samples.

We have prepared the composite films of these undoped, W-doped and W/Mg-codoped VO_2(M) on PET substrate with a commercial acrylic block copolymer. The copolymer in

***Table* 2.** The phase transition properties of the undoped, W-doped and W/Mg-codoped VO_2(M) measured from DSC and resistivity measurements

		Undoped	W-doped	W/Mg-codoped
T_c (°C)	DSC	63	35	44
	Resistivity	70	43	50
ΔT	DSC	4.3	12	8.5
	Resistivity	7.5	10.1	11.8

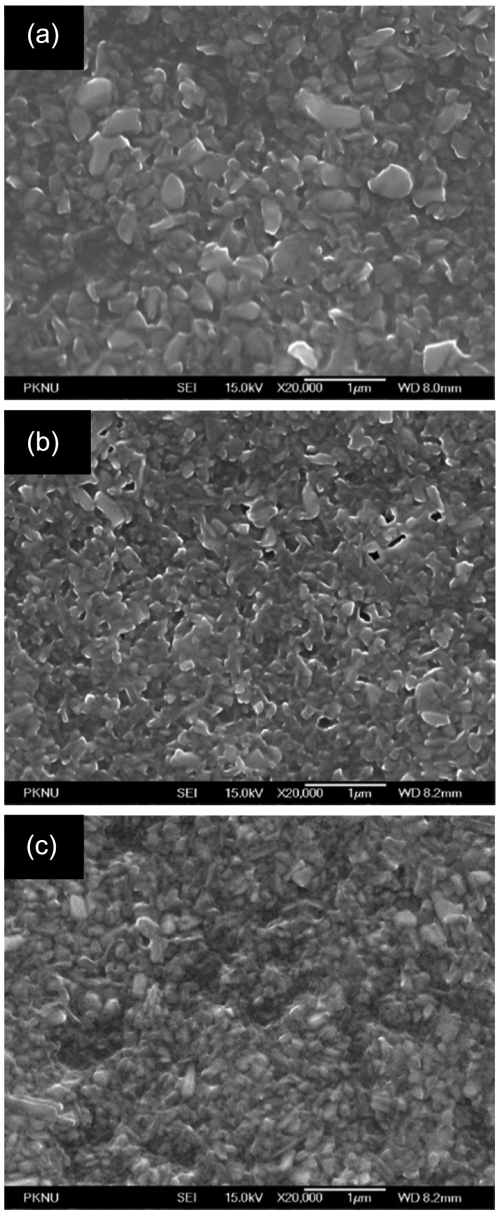

***Figure* 7.** FE-SEM images of (a) the undoped, (b) W-doped and (c) W/Mg-codoped VO_2(M) composite films on PET substrate (Magnification: x20,000).

the film plays a role of binder as well as dispersing agent during preparation of coating solution. The film thicknesses of all the samples were almost same as about 150 nm. The microscopic morphologies of these films were taken by FE-SEM and shown in *Fig.* 7. There were no cracks and the surfaces were all rough and porous for all three samples. The aggregated surface particles in the undoped sample were the largest while both the doped ones had slightly smaller and similar size. This is consistent with the aggregated particle sizes of the powder samples shown in *Fig.* 3.

The W/Mg-codoped composite film had the least haze among three types of films when they were prepared at the same condition. This means that the solvent dispersibility of W/Mg-codoped VO_2(M) was relatively better than those of the undoped and W-doped ones. The visible and near-infrared (NIR) spectra of these films depending on temperature were measured for the wavelengths of 350–

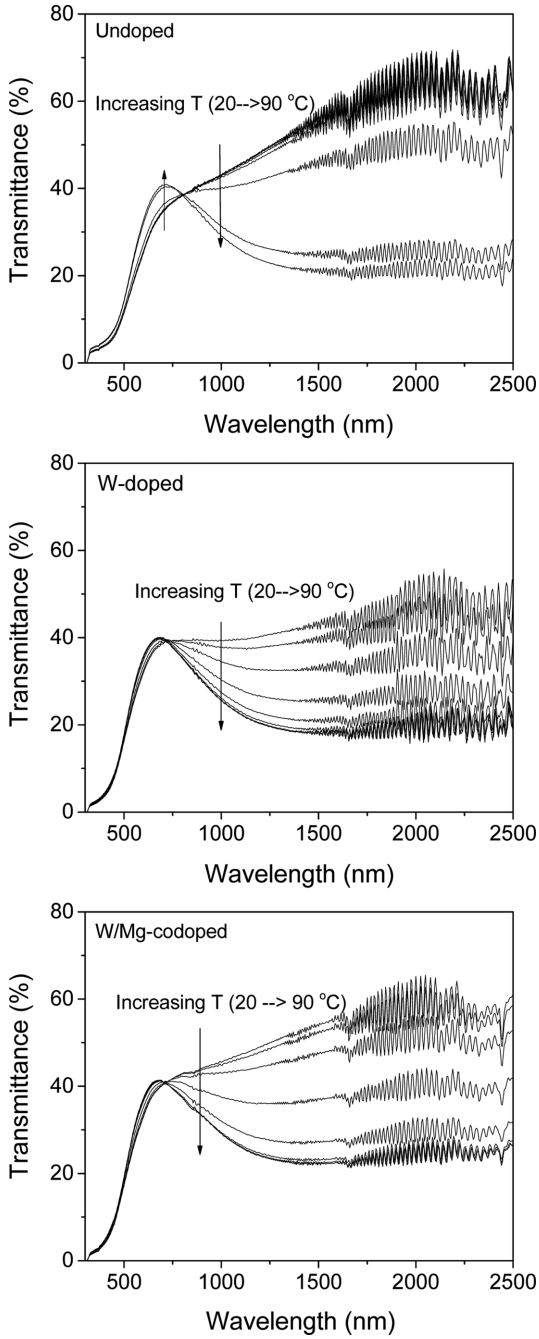

***Figure* 8.** Temperature dependence of transmission spectra of the undoped, W-doped and W/Mg-codoped VO_2(M) composite films on PET substrate.

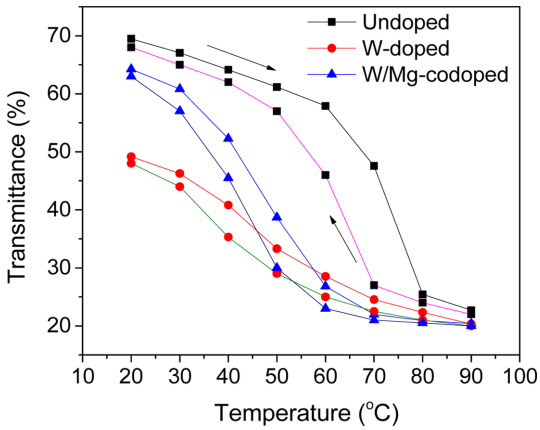

***Figure* 9.** Temperature dependence of transmittances at 2,000 nm for the undoped, W-doped and W/Mg-codoped VO_2(M) composite films on PET substrate.

***Table* 3.** Optical transition properties of the undoped, W-doped and W/Mg-codoped VO_2(M) composite films on PET substrate

		Undoped	W-doped	W/Mg-codoped
T_c (°C)		67	42	44
ΔT_c (°C)		11	7	5
Transmittance	20 °C	69.5	49.2	64.2
at 2000 nm T (%)	90 °C	22.7	20.3	21.4
ΔT (%)		46.8	28.9	42.8

2,500 nm and the temperature range of 20–90 °C and shown in *Fig*. 8. As you can see in the figures, the thermochromic characteristics were clearly shown as the temperature changed. The NIR transmittance of all three films decreased as temperature increased while the visible transmittance slightly increased oppositely. In *Fig.* 9 the transmittance-vs-temperature curves at 2,000 nm were plotted for all three films. The transmittance change (ΔT) between 20 °C and 90 °C was most pronounced for the undoped film as 47% and it decreased to 29% for the W-doped film. But it increased back to 43% for the W/Mg-codoped film. The transition temperatures that were determined from the transmittance data during heating and cooling cycles were 67, 42, 44 °C for the undoped, W-doped and W/Mg-codoped films, respectively. This tendency is also consistent with the data of powder and pellet samples from DSC and resistivity as discussed above. The hysteresis during heating and cooling became narrower for both the doped films than for the undoped one. This is opposite result to that of the powder and pellet samples. The same hysteresis tendency was shown for the W-doped and W/Mg-codoped films that was prepared by the precursor sol-gel method that was mentioned in Introduction. This difference between the powder and film samples may result from the fact that the grain size effect in film sample is more serious than powder sample.[20] As mentioned earlier Mg-doping improved the visible transmittance of VO_2(M) films and the result was explained due to the band-gap widening whether it is singly doped or codoped with W. In our composite film Mg-codoping into VO_2(M) with W did not show the pronounced effect on the visible transmittance as shown in *Fig*. 8 although there was very slight improvement. Rather than this, as discussed above, Mg-codopoing apparently recovered the deteriorated transition characteristics by W-doping and NIR transmittance change after the transition, which is called as NIR switching efficiency, was recovered to the level of the undoped VO_2(M) while keeping the transition temperature low. Therefore, this study showed that the Mg-codoping effect in W-doped VO_2(M) nanoparticle played more important role on the structural phase transition than band gap widening that were shown in the other study of W/Mg-codoped film.

CONCLUSION

W-doping into VO_2(M) gives definitely a benefit of lowering the phase temperature as well known. However, it also causes the lowering of the sharpness of the phase transition and decreases the NIR switching efficiency. Mg-codoping into W-doped VO_2(M) nanoparticles synergistically increased the transition sharpness back to the level of the undoped VO_2(M) while keeping the transition temperature low. The W/Mg-codoped VO_2(M) composite film that was prepared with W(1.5 at. %)/Mg(2.9 at. %)-codoped nanoparticles and acrylic block copolymer showed relatively low transition temperature (44 °C) and good NIR switching efficiency (43%). The optimization of this synergistic effect is under investigation by controlling W/Mg-codoping ratio.

Acknowledgments. This work was supported by a Research Grant of Pukyong National University (Year 2015).

REFERENCES

1. (a) Kamalisarvestani, M; Saidur, R.; Mekhilef, S.; Javadi, F. S. *Ren. Sust. Ener. Rev.* **2013**, *26*, 353. (b) Gao, Y.; Luo, H.; Zhang, Z.; Kang, L.; Chen, Z.; Du, J.; Kanehira, M.; Cao, C. *Nano Ener.* **2012**, *1*, 221. (c) Granqvist, C. G.; Lansaker, P. C.; Mlyuka, N. R.; Niklasson, G. A.; Avendano, E. *Sol. Energy. Mater. Sol. Cells* **2009**, *93*, 2032.
2. Morin, F. *J. Phys. Rev.* **1959**, *3*, 34.
3. Takei, H.; Koide, S. *J. Phys. Soc. Japan* **1966**, *21*, 1010.
4. Koide, S.; Takei, H. *J. Phys. Soc. Japan* **1967**, *22*, 946.

5. Livage, J. *Solid State Ionics* **1996**, *86*, 935.
6. Dachuan, Y.; Niankan, X.; Jingyu, Z.; Xiulin, Z. *J. Phys. D: Appl. Phys.* **1996**, *29*, 1051.
7. Fuls, E. N.; Hensler, D. H.; Ross, A. R. *Appl. Phys. Lett* **1967**, *10*, 199.
8. (a) Goodenough, J. B. J. Solid State Chem. **1971**, *3*, 490. (b) Beteile, F.; Livage, J. *J. Sol-Gel Sci. Technol. 1998*, *13*, 915.
9. (a) Horlin, T.; Nikelwski, T.; Nygren, M. *Mat. Res. Bull.* **1972**, *7*, 1515. (b) Tang, C; Georgopoulos, P.; Fine, M. E. Cohen, J. B. *Phys. Rev. B* **1985**, *15*, 31. (c) Sobhan, M. A.; Kivaisi, R. T.; Stjerna, B.; Granqvist, C. G. *Sol. Energy Mater. Sol. Cells* **1996**, *44*, 451. (d) Li, G.; Chao, K.; Peng, H.; Chen, K.; Zhang, Z. *Inorg. Chem.* **2007**, *46*, 5787.
10. (a) Burkhardt, W.; Christmann, T.; Meyer, B. K.; Niessner, W.; Schalch, D.; Scharmann, A. *Thin Solid Films* **1999**, *345*, 229. (b) Kiri, P.; Warwick, M. E. A.; Ridley, I.; Binions, R. *Thin Solid Films* **2011**, *520*, 1363. (c) Dai, L.; Chen, S.; Liu, J.; Gao, Y.; Zhou, J.; Chen, Z.; Cao, C.; Luo, H.; Kanehira, M. *Phys. Chem. Chem. Phys.* **2013**, *15*, 11723.
11. (a) Mlyuka, N. R.; Niklasson, G. A.; Granqvist, C. G. *Appl. Phys. Lett.* **2009**, *95*, 171909. (b) Li, S.-Y.; Mlyuka, N. R.; Primetzhofer, D.; Hallen, A.; Possnert, G.; Niklasson, G. A. Granqvist, C. G. *App. Phys. Lett.* **2013**, *103*, 161907. (c) Zhou, J.; Gao, Y.; Liu, X.; Chen, Z.; Dai, L.; Cao, C.; Luo, H.; Kanahira, M.; Sun, C.; Yan, L. *Phys. Chem. Chem. Phys.* **2013**, *15*, 7505.
12. (a) Takahashi, I.; Hibino, M.; Kudo, T. *J. Appl. Phys.* **2001**, *40*, 1391. (b) Burkhardt, W.; Christmann, T.; Franke, S.; Kriegseis, W.; Meister, D.; Meyer, B. K.; Niessner, W.; Schalch, D.; Scharmann, A. *Thin Solid Films* **2002**, *402*, 226. (c) Soltani, M.; Chaker, M.; Haddad, E.; Kruzelecky, R. V.; Margot, J. *Appl. Phys. Lett.* **2004**, *85*, 1958. (d) Jiazhen, Y.; Yue, Z.; Wanxia, H. *Thin Solid Films* **2008**, *516*, 8554. (e) Kong, F. Y.; Li, M.; Zhang, J.; Xu, Y.; Li, D. B.; Zeng, Z.; Li, G. H. *Open J. of Adv. Mater. Res.* **2013**, *1*, 1.
13. Wang, N.; Liu, S.; Zeng, X. T.; Magdassi, S.; Long, Y. *J. Mater. Chem. C* **2015**, *3*, 6771.
14. (a) Alie, D; Gedvilas, L.; Wang, Z.; Tenent, R.; Engtrakul, C.; Yan, Y.; Shaheen, S. E.; Dilon, A. C.; Ban, C. *J. Solid State Chem.* **2014**, *212*, 237. (b) Ji, S.; Zhao, Y.; Zhang, F.; Jun, P. *J. Crys. Growth* **2010**, *312*, 282, (c) Ji, S.; Zhang, F.; Jin, P. *Res. Chem. Intermed*. **2011**, *37*, 493. (d) Zhang, Y.; Zhang, J.; Zhang, X.; Deng, Y.; Zhong, Y.; Huang, C.; Liu, X.; Liu, X.; Mo, S. *Ceram. Int.* **2013**, *39*, 8363.
15. (a) Zhang, K.-F.; Liu, X.; Su, Z.-X.; Li, H.-L. *Mater. Lett*. **2007**, *61*, 2644, (b) Liu, X.; Xie, G.; Huang, C.; Xu, Q.; Zhang, Y.; Luo, Y. *Mater. Lett.* **2008**, *62*, 1878, (c) Li, G.; Chao, K.; Peng, H.; Chen, K.; Zhang, Z. *Inorg. Chem*. **2007**, *46*, 5787.
16. JCPDS 81-2392.
17. JCPDS 43-1051, 72-0514, 82-0661.
18. (a) Horlin, T.; Niklewski, T.; Nygren, M. *Mater. Res. Bull.* **1973**, *8*, 179. (b) Parkin, I.; Manning, T. D. J. Chem. Educ. 2006, 83, 393. (c) Chae, B. G.; Kim, H. T.; Yun, S. *J. Electrochem. Solid-State Lett.* **2008**, *11*, 53.
19. Lopez, R.; Haynes, T. E.; Boatner, L. A.; Feldman, L. C.; Haglund, R. F. *Phys. Rev. B: Condens. Matter*, **2002**, *65*, 224113.
20. Verleur, H.; Barker, A. Berglund, C. *Phys. Rev.* **1968**, *172*, 788.